MAVEN observation of magnetosonic waves in the Martian magnetotail region

ShangChun Teng[1*], JiCheng Sun[2], JiaWei Gao[3,4], Y. Harada[5], Markus Fraenz[6], and DeSheng Han[1]

[1]State Key Laboratory of Marine Geology, School of Ocean and Earth Science, Tongji University, Shanghai 200092, China;

[2]MNR Key Laboratory for Polar Science, Polar Research Institute of China, Shanghai 200136, China;

[3]Key Laboratory of Earth and Planetary Physics, Institute of Geology and Geophysics, Chinese Academy of Sciences, Beijing 100029, China;

[4]College of Earth and Planetary Sciences, University of Chinese Academy of Sciences, Beijing 100049, China;

[5]Department of Geophysics, Kyoto University, Kyoto, Japan;

[6]Max-Planck-Institute for Solar System Research, Goettingen, Germany

Key Points:
- Magnetosonic waves were observed in the Martian magnetotail region by MAVEN.
- Enhanced proton and oxygen fluxes may provide free energy for the generation of magnetosonic waves.
- Cyclotron heating by magnetosonic waves may facilitate the Martian ionospheric proton escape.

Citation: Teng, S. C., Sun, J. C., Gao, J. W., Harada, Y., Fraenz, M., and Han, D. S. (2024). MAVEN observation of magnetosonic waves in the Martian magnetotail region. *Earth Planet. Phys.*, *8*(2), 317–325. http://doi.org/10.26464/epp2024003

Abstract: Magnetosonic waves are an important medium for energy transfer in collisionless space plasma. Magnetosonic waves have been widely investigated in the upstream of the bow shock at Mars. These waves are believed to originate from pickup ions or reflected particles. By utilizing MAVEN spacecraft data, we have observed the occurrence of quasi-perpendicularly propagating magnetosonic emissions near the proton gyrofrequency in the Martian magnetotail region. These plasma waves are associated with a significant enhancement of proton and oxygen flux. The excited magnetosonic waves could possibly heat the protons through resonance and facilitate the ionospheric plasma escape. Our results could be helpful to better understand the Mars' magnetospheric dynamics and offer insights into possible energy redistribution between waves and plasma in the Martian nightside magnetosphere.

Keywords: Martian magnetotail region; magnetosonic waves; proton escape

1. Introduction

Magnetosonic waves, also referred to as equatorial noise and ion Bernstein modes, have been extensively observed in Earth's magnetosphere (Chen L and Thorne 2012; Tsurutani et al. 2014; Balikhin et al. 2015; Boardsen et al. 2016; Yao F et al. 2020). These waves play a fundamental role in the energy transfer process of collisionless space plasma (Shprits 2009; Bortnik and Thorne 2010; Li J et al. 2016; Ni BB et al. 2018). It is commonly believed that magnetosonic waves grow from the free energy of ring current protons with ring-distribution (Boardsen et al. 1992; Min K et al. 2018; Teng S et al. 2021). Through resonant and nonresonant interactions, magnetosonic waves heat plasmaspheric ions (Yuan Z et al. 2018) and accelerate and scatter radiation belt electrons (Horne et al. 2007; Shprits 2016), making them essential for energy transfer in Earth's magnetosphere. Additionally, magnetosonic waves have also been observed on Mars (Bertucci et al. 2004; Collinson et al. 2018; Harada et al. 2019).

The absence of a global dipole magnetic field on Mars, with only localized crustal magnetic fields, has prompted a growing interest in investigating magnetosonic waves in its magnetosphere (Øieroset et al. 2004; Langlais et al. 2004, 2019, 2020, Wang J et al. 2021). The interaction between Mars' ionosphere and the solar wind creates distinct regions, including a bow shock, magnetosheath, induced magnetosphere, and ionosphere (Acuña et al. 1998; Nagy et al. 2004). Recently, there has been growing attention towards studying magnetosonic waves at Mars due to their potential impact on plasma heating and loss within the Martian ionosphere (Espley 2004; Ergun et al. 2006; Fowler et al. 2018), as well as their significance in the process of Martian atmospheric escape (Wei HY et al. 2011). A study by Su Z et al. (2020) demonstrates that magnetosonic waves can heat the topside ionospheric electrons through the Landau resonance, resulting in the enhancement of the ambipolar electric potential and facilitating the escape of ionospheric plasma. Previous statistical analyses indicate that magnetosonic waves are most frequently observed in the upstream region of the Martian bow shock (Wei HY et al. 2014; Fowler et al. 2018; Liu D et al. 2020). The exact mechanism of generating waves with different properties remains elusive. A commonly proposed explanation suggests that these waves are

generated by the newly ionized particles of the solar wind near the upstream parallel foreshock and subsequently propagate through the magnetosheath into the ionosphere (Russell et al. 1990; Brain 2002; Collinson et al. 2018). Another possibility is that magnetosonic waves can be formed from ion beams reflected at the bow shock (Hoppe and Russell 1983; Wilson 2016). Wang J et al. (2023) has demonstrated that magnetosonic waves can also be locally generated by the ring-beam proton distributions of magnetosheath origin in the Martian ionosphere. The waves observed in the nightside of the Martian magnetosphere have received limited investigation. Fowler et al. (2021) reported the presence of magnetosonic waves in the Martian nightside magnetosphere. These waves are proposed to be generated by solar wind pressure pulses and to propagate into the nightside ionosphere due to the draped interplanetary magnetic field (IMF). Additionally, Guo Z et al. (2022) reported the existence of lower hybrid drift waves in the Martian magnetotail and suggested that the proton density gradient potentially excite the lower hybrid drift instability.

This study investigates magnetosonic waves in the Martian magnetotail region and focuses on two representative events with similar characteristics. Through the measurements of field and particle, we propose the potential generation mechanisms of these waves. Their potential effects on plasma heating and escape are also discussed. By exploring their origins, wave characteristics and potential impacts, we seek to broaden our understanding of the dynamic process between these waves and the surrounding plasma environment.

2. Observations

The data utilized in this study comprise magnetic field and plasma measurements obtained from Mars Atmosphere and Volatile EvolutioN (MAVEN) mission (Jakosky et al. 2015). MAVEN operates in an elliptical orbit with a periapsis at ~150 km and an apoapsis at ~6000 km. The magnetic field data were acquired by the Magnetometer instrument (MAG) at a sampling rate of 32 Hz (Connerney et al. 2015). Solar Wind Ion Analyzer (SWIA) (Halekas et al. 2015) provides energy spectrum and angular distribution measurement of solar wind and magnetosheath ions in the energy range of 5 eV to 25 keV. The electron density data was obtained from the Solar Wind Electron Analyzer (SWEA) data (Mitchell et al. 2016). The SWEA measures suprathermal electrons at energies above 3 eV, thus the corresponding electron density is for electrons over 3 eV. The SupraThermal and Thermal Ion Composition (STATIC) instrument (McFadden et al. 2015) supplies energy-angular distributions of suprathermal and thermal ions including H^+, He^{++}, O^+, O_2^+ and CO_2^+. Two representative events with similar characteristics will be analyzed in this article.

2.1 Event 1: May 9, 2015

The first typical event focuses on the time of the occurrence of magnetosonic waves. Figures 1a–b depict a map of MAVEN orbit No.1180 on May 09 2015, in the right-handed Mars-Sun-Orbit (MSO) frame, viewed from different planes. In this coordinate system, the x axis points toward the Sun, the y axis points backwards along the tangent of Mars' orbit and the z axis completes the right-handed system. The boundaries of the bow shock and

Magnetic Pileup Boundary (dashed lines) are determined based on Vignes et al. (2000). During this orbit, the spacecraft passed its periapsis at 17:08 UT and at an altitude of 162 km. Between 17:25 and 18:34 UT, it traversed the magnetosheath region. Magnetosonic waves were observed during the time interval of 16:18–16:33 UT. The corresponding spacecraft orbit during this period is highlighted in blue in Figures 1a–b, with an altitude range of ~3000−2000 km and Solar Zenith Angle (SZA) varying from ~130° to 120° so that the data set covers the nightside sector (SZA > 90°).

During the selected time interval, we analyzed the wave properties detected by MAVEN MAG (Magnetometer) in Figures 1c–k. The occurrence of magnetosonic waves within this interval (16:18–16:33 UT) is denoted by two dashed magenta lines, corresponding to the blue dots in Figures 1a–b. Figure 1c displays the magnetic field components in the Mars-Sun-Orbit (MSO) coordinate system, showing minimal variation in the magnetic field magnitude around 10 nT, with the field primarily oriented along the −x direction. We transformed the magnetic field into the Field Aligned Coordinate (FAC) system, where the magnetic field points along the z axis from 16:10 to 16:49 UT in Figure 1d. The waves are predominantly represented by the compressional component of the magnetic field, and the wave magnitude dB/B reaches 0.05. For further examination, we conducted a wave polarization analysis using the method by Means (1972). Figures 1e–h present the total wave power, degree of polarization, wave normal angle, and ellipticity as functions of time and frequency. Only the bins where the magnetic field wave power is larger than the background noise by at least one order of magnitude are shown. The observed waves occur near the local proton cyclotron frequency (f_{cp}) (~0.2 Hz), with a second harmonic structure at a frequency of ~0.4 Hz (Figure 1e). The wave degree of polarization exceeded 80% (Figure 1i), indicating coherent signals at the relevant frequencies and validating the wave polarization calculation results. The wave normal angle is notably large (> 80°) (Figure 1j), suggesting quasi-perpendicular propagation. The ellipticity (Figure 1k) predominantly fluctuates around 0, indicating predominantly linear and right-handed polarization. These characteristics are consistent with magnetosonic waves, which exhibit compressive behavior and linear right-handed polarization, differing from ion cyclotron waves that are primarily dominated by the transverse component and exhibit left-handed polarization. Magnetosonic waves with similar properties are discussed in Fowler et al. (2018), but on the dayside. Magnetosonic waves here are electromagnetic emissions with frequencies between the proton gyrofrequency and the lower hybrid resonance frequency. It is different from the classic MHD wave mode, which are usually observed in the ultra-low frequency domain (Ruhunusiri et al. 2015).

Figure 2 presents the time series of particle measurements. Figures 2a and 2b display the ion mass spectra and energy spectra observed by STATIC, facilitating the determination of ion composition through the mass-time spectrogram (Figure 2a). During the wave occurrence period, there is a prominent increase in H^+, He^+, O^+, and O_2^+ energy fluxes. Detailed energy spectra for H^+ and O^+ are depicted in Figures 2c and 2d, respectively, showing intensified energy fluxes of H^+ around ~10 eV. The velocity of H^+ and O^+ is presented in Figures 2e and 2h. Figure 2g shows the temperature
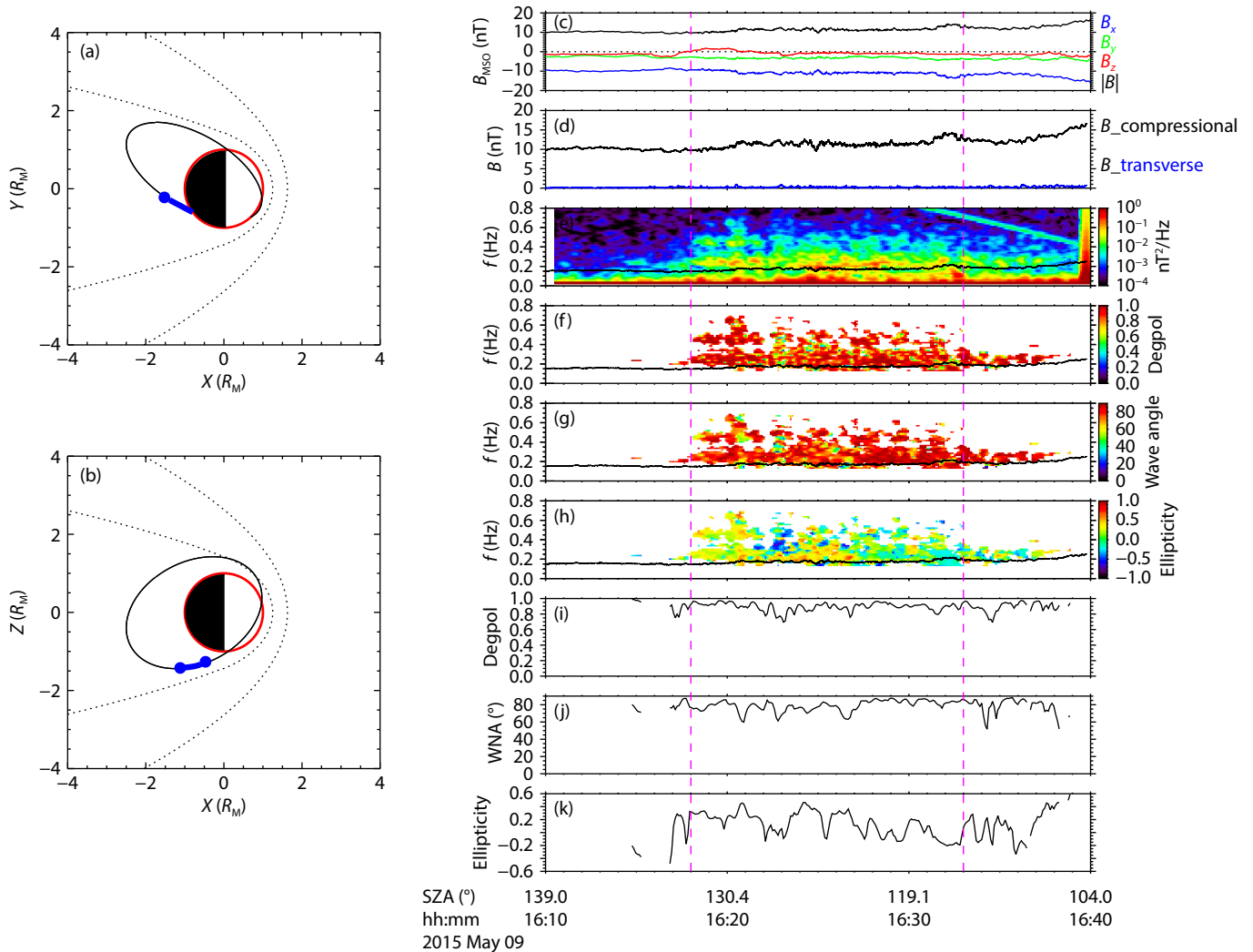
Figure 1. MAVEN observations during 16:10–16:40 UT on 9 May 2016. (a, b) MAVEN orbit in MSO coordinate viewed from different planes. The satellite trajectory when the waves occur are marked by the blue lines. The blue dots correspond to the time denoted by the vertical magenta lines in Figures 1c–k. The black dashed lines are the bow shock and magnetic pileup boundary which separates the magnetosheath and magnetic pileup region. Units are in planetary radii, where R_M = 3390 km. (c) MAVEN magnetic field components in MSO coordinates. Magnetic field B_x, B_y and B_z and magnitude $|B|$ are shown in blue, green, red, and black. (d) The compressional and transverse component of magnetic field. (e) The total wave power spectral density. (f) The degree of polarization. (g) The wave normal angle. (h) The wave ellipticity. In Figures 1e–h, the black line denotes the proton frequency (f_{cp}). Figures (i)–(k) show the weighted average value of degree of polarization (i), wave normal angle (j) and ellipticity (k). The vertical magenta dashed lines indicate the times of the wave analyzed by this study.

of H$^+$. The velocity and temperature of H$^+$ outside the magenta lines is not valid, as STATIC does not observe significant numbers of protons in that region.

Previous studies have demonstrated that the wave characteristics observed at Mars may be influenced by Doppler shift effects (Brain 2002). To account for these effects and obtain meaningful wave characteristics, we utilized the Doppler shift relation (Jian LK et al. 2009, 2010) to quantify the Doppler shift corrections.

$$f_{bf} = f_{obs} + \frac{\boldsymbol{k} \cdot \boldsymbol{V}_{bf}}{2\pi} = f_{obs}\left(1 + \frac{V_{bf}}{V_A}\hat{\boldsymbol{k}} \cdot \hat{\boldsymbol{V}}_{obs}\right), \qquad (1)$$

where f_{obs} is the observed wave frequency, f_{bf} is the wave frequency for bulk flow frame after removing Doppler shift, $\boldsymbol{k}$ is the wave propagation vector, $\hat{\boldsymbol{k}}$ represents the unit vector, $\boldsymbol{V}_{bf}$ is the oxygen bulk flow velocity, V_A is the Alfven speed, and $\hat{\boldsymbol{V}}_{obs}$ is

the observed oxygen bulk flow velocity. During this interested time interval, we assume the oxygen ions are dominated. For the magnetosonic waves except near the cutoff frequency, the dispersion relation can be approximately described as $\omega \approx k_\perp V_A$, thus a simple estimate of the magnetosonic wavelength is obtained via $\lambda = V_A/f$, where f = 0.2 Hz, V_A is calculated using the observed magnetic field strength and oxygen density (~3.6 cm^{-3}). V_{bf}/V_A is estimated to be ~0.23 and $\hat{\boldsymbol{k}} \cdot \hat{\boldsymbol{V}}_{bf}$ is nearly 0. Compared with 1, the second term in Equation (1) is small. Consequently, the Doppler shift effects due to oxygen bulk velocity are not significant in this case.

2.2 Event 2: April 24, 2015

Through our examination of the wave observations from MAVEN, we have identified another wave event exhibiting similar charac-
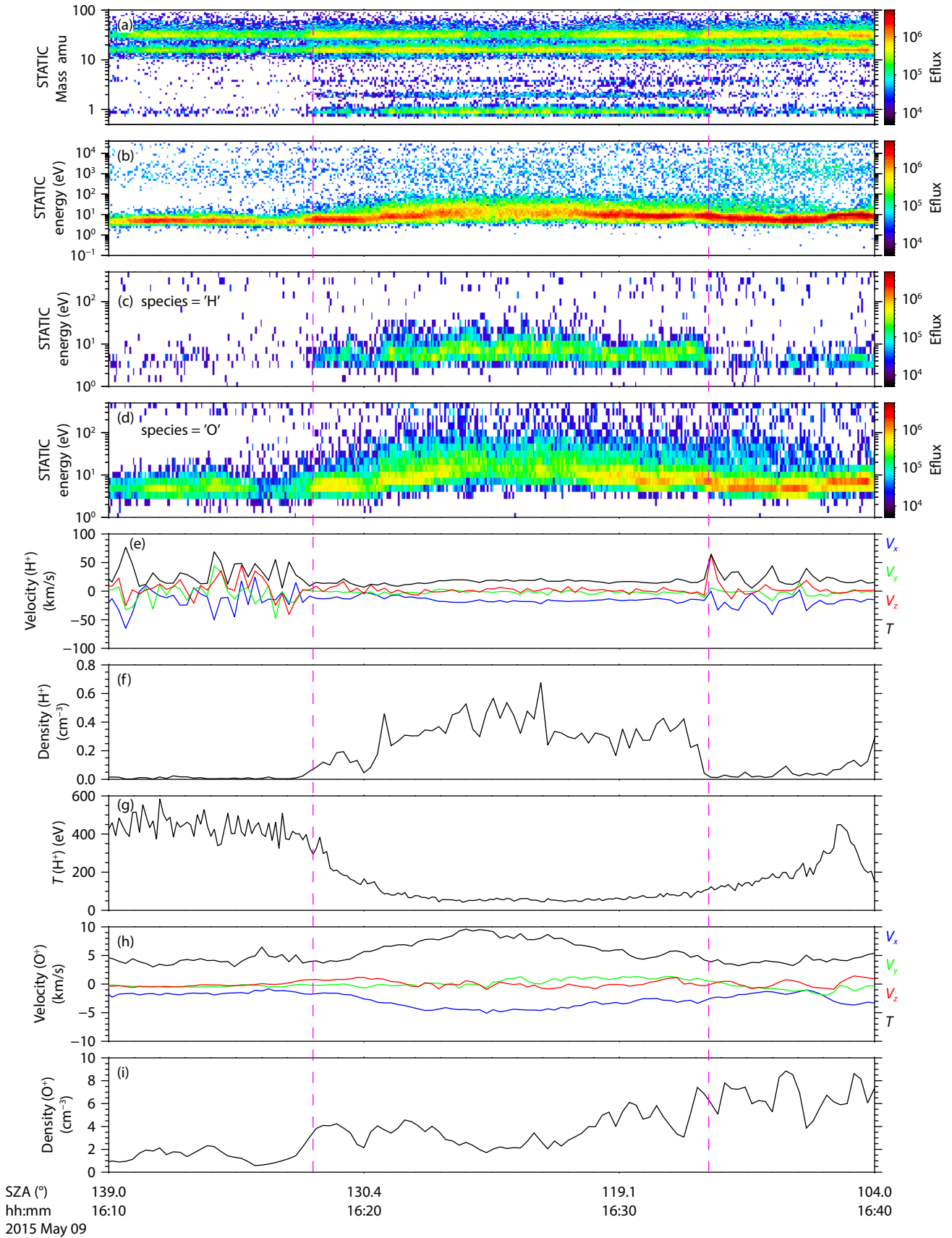
Figure 2. Time series of plasma data. (a) SupraThermal and Thermal Ion Composition mass spectra; (b) Omnidirectional energy spectra; (c) H^+ energy flux; (d) O^+ energy flux; (e) The velocity of H^+; (f) The density of H^+; (g) The temperature of H^+; (h) The velocity of O^+; (i) The density of O^+. Magenta vertical lines mark time intervals that magnetosonic waves were observed.
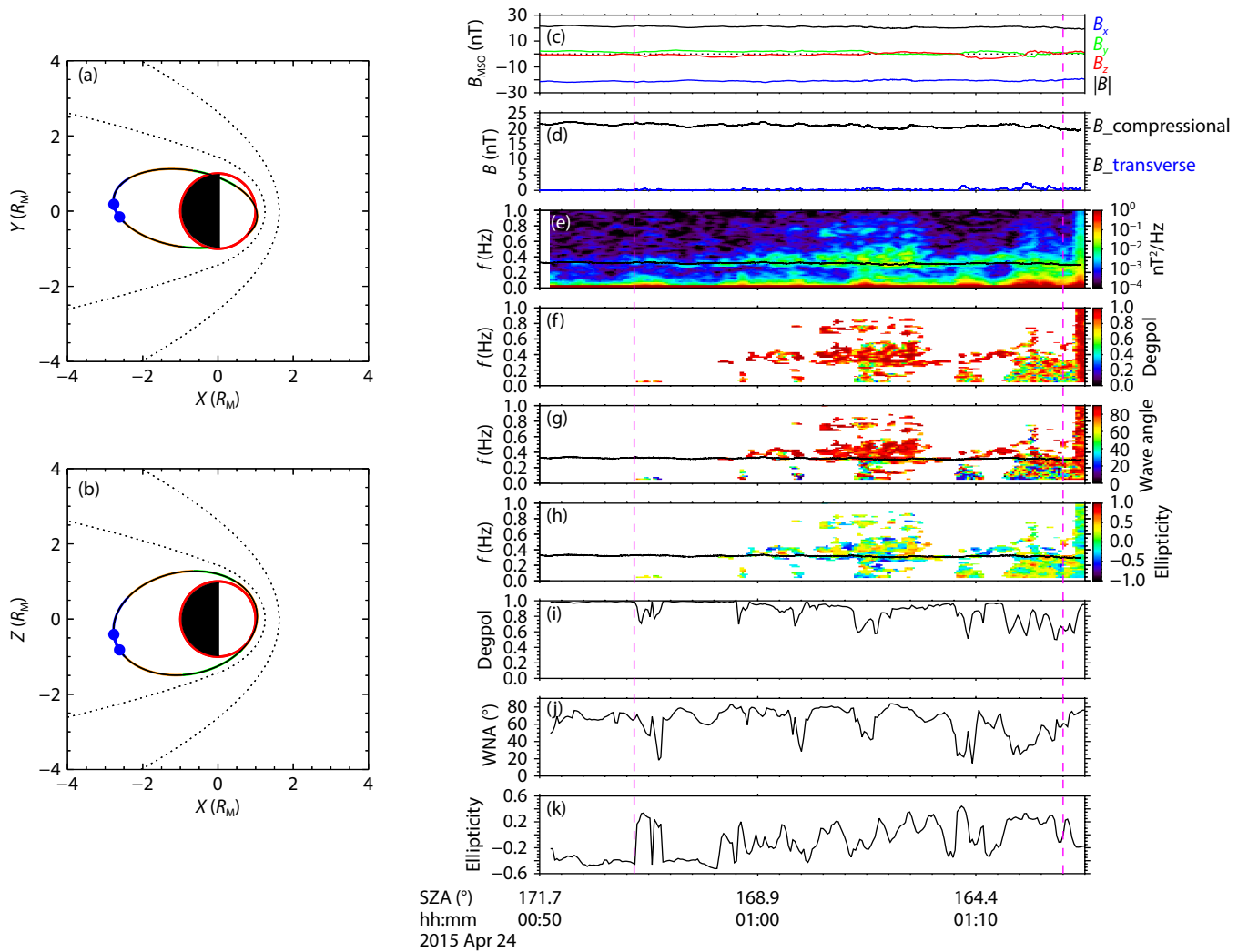
Figure 3.   The region in which the waves are observed and wave polarized characteristics. This figure has the same format with Figure 1.

teristics. Figure 3 displays the MAVEN location where the waves occurred and the corresponding wave characteristics, following the same format as Figure 1. Compared with Event 1, this event was observed at an altitude of approximately 6000 km, situated farther away from Mars and close to the apogee of the orbit. Figure 3c presents the three components of the magnetic field, with the magnetic fields further decomposed into field-aligned and perpendicular components in Figure 3d. Our analysis reveals that the compressional component of the magnetosonic waves predominates. Employing the Means method (Means 1972), we conducted polarization analyses of these waves as depicted in Figures 3c–k. The waves were observed between ~00:54 and 01:14 UT, marked by vertical magenta dashed lines. The magnetic field spectrogram in Figure 3e indicates the main wave intensity around the proton gyrofrequency (f_{cp}), represented by the black line. A noticeable increase in wave intensity is also observed around $2f_{cp}$, indicating a harmonic structure. Figures 3f–h show the wave degree of polarization, wave normal angle, and wave ellipticity, respectively. Their corresponding weighted average values are presented in Figures 3i–k. Notably, the degree of polarization values are close to 1, affirming the validity of these polarization parameters. The wave normal angle values vary above 60°, suggesting predominantly quasi-perpendicular propagation. The

ellipticity values fluctuate between −0.5 and 0.5, indicating nearly linear polarization. These features align with the properties expected for magnetosonic waves.

Figure 4 presents an overview of the plasma during the wave observation. The panels from top to bottom display the ion mass spectra (a), ion energy spectra (b), proton energy spectra (c), oxygen energy spectra (d), proton velocity (e), proton density (f), the proton temperature (g), oxygen velocity (h) and oxygen density (i) respectively. The velocity of H^+ is very small, indicating the magnetotail region. The energy spectra of ions indicate that H^+ dominates at energies of approximately 10 eV, while O^+ dominates at energies of approximately 10−100 eV during the magnetosonic wave observations. Additionally, O^+ and O_2^+ exhibit similar energy spectra. The temperature of H^+ increases during the period of time when the wave intensity increases. Both of the above two events indicate that during periods of enhanced waves, there is a significant increase in the energy flux of H^+. Li XZ et al. (2023) investigated the two types of Martian Magnetotail current sheets and the results suggest that the current sheet is dominated by either planetary heavy ions or H^+. The heavy ions in the tail current sheet originate from the Martian ionosphere. The detected H^+ is several tens of eV, possibly originating from the
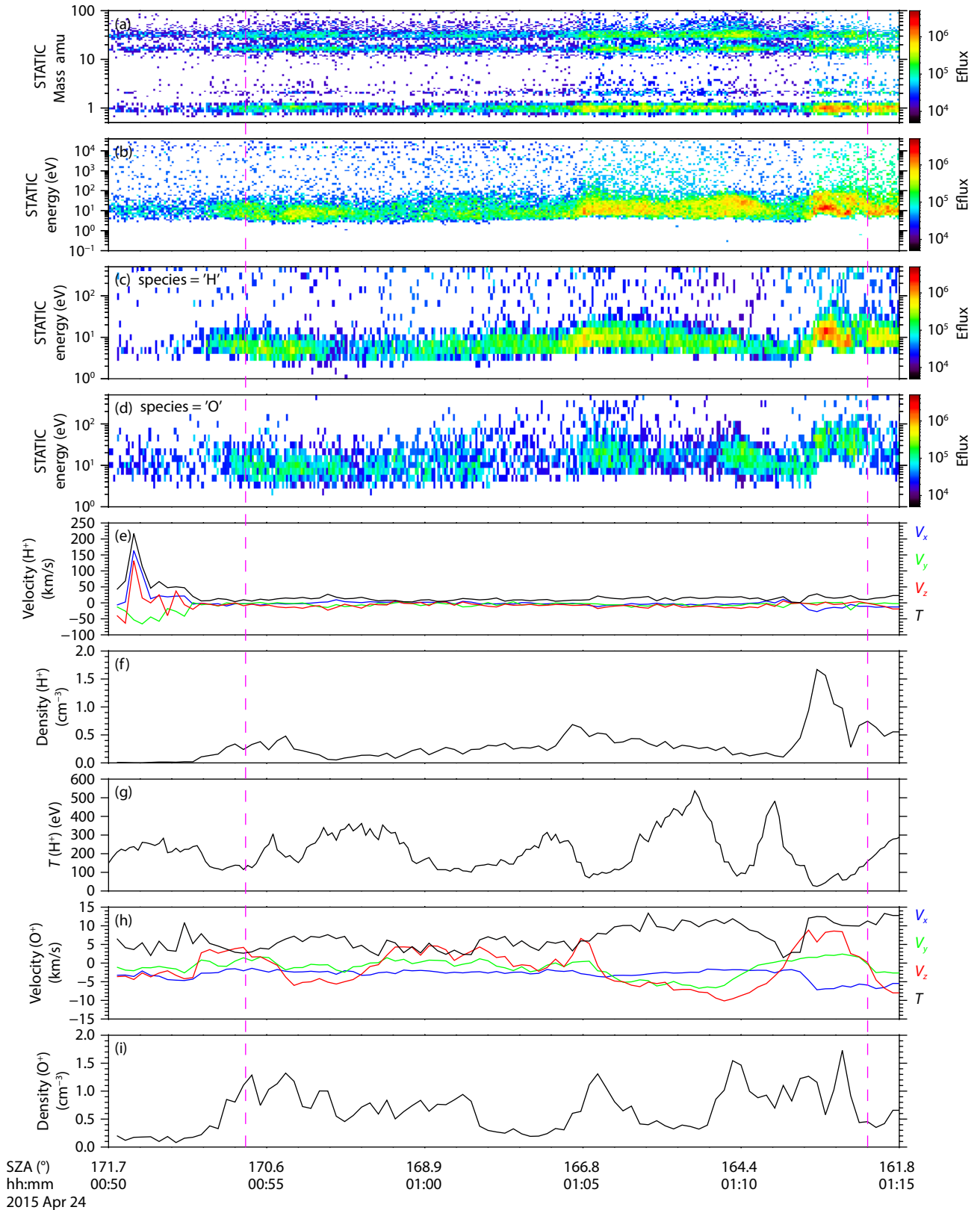
Figure 4. Particle characteristics for the observed event. This figure has the same format with Figure 2.

ionosphere.

3. Discussion

Magnetosonic waves play a crucial role in energy transfer, making

it essential to investigate their distribution, generation, and effects. Prior studies at Mars have observed ion cyclotron waves with frequencies close to or below the local f_{cp}. These waves exhibit left-handed elliptical polarization, propagating parallel to

the magnetic field as transverse waves, typically generated by ion instabilities from pickup ions or back streaming ions, and are mainly observed in the upstream foreshock region. In contrast, the waves reported in this study exhibit two distinct features different from past studies: (1) the waves are present in the Martian magnetotail region, and (2) the wave polarization analysis indicates propagation quasi-perpendicular to the background magnetic field. Based on these observed wave properties, they are categorized as magnetosonic waves, distinguishing them from ion cyclotron waves.

With the suite of particle instruments onboard MAVEN, we propose two potential generation mechanisms for the observed magnetosonic waves. Firstly, the presence of a ring-like proton distribution could provide free energy for the wave generation. Previous studies (Wang J et al. 2023) proposed that magnetosonic waves in the Martian dayside ionosphere are locally generated by ring beam hot protons resulting from the penetration of solar wind protons. Similarly, in the nightside of the magnetotail region, the presence of an unstable warm proton distribution could lead to proton Bernstein mode instability (Boardsen et al. 2015; Harada et al. 2019). Secondly, the ion Bernstein instability driven by ring-like O^+ distributions with a positive gradient can also excite O^+ Bernstein waves (Min K et al. 2017; Liu K et al. 2020). While magnetosonic waves can be unstable over a broad range of continuous frequencies, the peak of the growth rate typically falls within the frequency range of $10-30 f_{cp}$ (Liu K et al. 2011; Chen L et al. 2016). The wave frequency in this case is close to f_{cp}, it remains possible that ring-like O^+ distributions excite these waves. The specific source and formation mechanism of the waves require further investigation, as the observed particle distribution data varies significantly at each moment, making it challenging to obtain precise particle distribution information.

Previous studies have extensively investigated the contributions of magnetosonic waves to ionospheric particles through resonant interaction and adiabatic compression processes (Collinson et al. 2018; Fowler et al. 2018). Fowler et al. (2020) proposed that a combination of the adiabatic magnetic pumping and the pitch angle scattering could heat the ionospheric suprathermal electrons. Additionally, Akbari et al. (2019) has highlighted the fundamental role of plasma waves in coupling the solar wind and planetary plasma. The close relationship between H^+ enhancement and wave occurrence suggests a region of plasma heating. The magnetosonic waves with frequencies approaching f_{cp} can heat cool background protons to tens of eV through cyclotron or Landau resonance (Ma Q et al. 2019; Teng S et al. 2019; Su Z et al. 2020; Wu Z et al. 2022). The energy provided exceeds the escape energy of H^+, suggesting a potential mechanism for nightside ion escape where magnetosonic waves play a role in heating nightside H^+. The wave heating mechanism is crucial for ion outflow at Earth (Kintner et al. 1997), making the proposed Martian mechanism intriguing from the perspective of comparative planetology.

4. Conclusions

In this study, we analyzed magnetosonic waves observed in the Martian magnetotail region, with dominant frequencies around f_{cp} and harmonic structures at $2 f_{cp}$. These waves were characterized by a compressional component, quasi-perpendicular propaga-

tion, and linear polarization, leading to their identification as magnetosonic waves. Examining the plasma conditions, we found that these waves were accompanied by enhanced proton and oxygen fluxes. Through wave-particle interactions, the generated magnetosonic waves possibly in turn heat the proton species. These events provide a possible insight into understanding the physical process and plasma dynamics on the nightside of the Martian environment. Further investigations are required to fully quantify the energy transfer between magnetosonic waves and plasma. This study contributes to a deeper understanding of the dynamics of the Martian magnetosphere.

References

Acuña, M. H., Connerney, J. E. P., Wasilewski, P., Lin, R. P., Anderson, K. A., Carlson, C. W., McFadden, J., Curtis, D. W., Mitchell, D., … Ness, N. F. (1998). Magnetic field and plasma observations at mars: Initial results of the mars global surveyor mission. *Science*, *279*(5357), 1676–1680. https://doi.org/10.1126/science.279.5357.1676

Akbari, H., Andersson, L., Andrews, D. J., Malaspina, D., Benna, M., and Ergun, R. (2019). In situ electron density from active sounding: The influence of the spacecraft wake. *Geophys. Res. Lett.*, *46*(17-18), 10250–10256. https://doi.org/10.1029/2019GL084121

Balikhin, M. A., Shprits, Y. Y., Walker, S. N., Chen, L. J., Cornilleau-Wehrlin, N., Dandouras, I., Santolik, O., Carr, C., Yearby, K. H., and Weiss, B. (2015). Observations of discrete harmonics emerging from equatorial noise. *Nat. Commun.*, *6*, 7703. https://doi.org/10.1038/ncomms8703

Bertucci, C., Mazelle, C., Crider, D. H., Mitchell, D. L., Sauer, K., Acuña, M. H., Connerney, J. E. P., Lin, R. P., Ness, N. F., and Winterhalter, D. (2004). MGS MAG/ER observations at the magnetic pileup boundary of Mars: draping enhancement and low frequency waves. *Adv. Space Res.*, *33*(11), 1938–1944. https://doi.org/10.1016/j.asr.2003.04.054

Boardsen, S. A., Gallagher, D. L., Gurnett, D. A., Peterson, W. K., and Green, J. L. (1992). Funnel-shaped, low-frequency equatorial waves. *J. Geophys. Res.: Space Phys.*, *97*(A10), 14967–14976. https://doi.org/10.1029/92JA00827

Boardsen, S. A., Kim, E. H., Raines, J. M., Slavin, J. A., Gershman, D. J., Anderson, B. J., Korth, H., Sundberg, T., Schriver, D., and Travnicek, P. (2015). Interpreting ~1 Hz magnetic compressional waves in mercury's inner magnetosphere in terms of propagating ion-Bernstein waves. *J. Geophys. Res.: Space Phys.*, *120*(6), 4213–4228. https://doi.org/10.1002/2014JA020910

Boardsen, S. A., Hospodarsky, G. B., Kletzing, C. A., Engebretson, M. J., Pfaff, R. F., Wygant, J. R., Kurth, W. S., Averkamp, T. F., Bounds, S. R., … De Pascuale, S. (2016). Survey of the frequency dependent latitudinal distribution of the fast magnetosonic wave mode from Van Allen probes electric and magnetic field instrument and integrated science waveform receiver plasma wave analysis. *J. Geophys. Res.: Space Phys.*, *121*(4), 2902–2921. https://doi.org/10.1002/2015JA021844

Bortnik, J., and Thorne, R. M. (2010). Transit time scattering of energetic electrons due to equatorially confined magnetosonic waves. *J. Geophys. Res.: Space Phys.*, *115*(A7), A07213. https://doi.org/10.1029/2010JA015283

Brain, D. A., Bagenal, F., Acuña, M. H., Connerney, J. E. P., Crider, D. H., Mazelle, C., Mitchell, D. L., and Ness, N. F. (2002). Observations of low-frequency electromagnetic plasma waves upstream from the Martian shock. *J. Geophys. Res.: Space Phys.*, *107*(A6), SMP 9-1–SMP 9-11. https://doi.org/10.

1029/2000JA000416

Chen, L. J., and Thorne, R. M. (2012). Perpendicular propagation of magnetosonic waves. *Geophys. Res. Lett.*, *39*(14), L14102. https://doi.org/10.1029/2012GL052485

Chen, L. J., Sun, J. C., Lu, Q. M., Gao, X. L., Xia, Z. Y., and Zhima, Z. R. (2016). Generation of magnetosonic waves over a continuous spectrum. *J. Geophys. Res.: Space Phys.*, *121*(2), 1137–1147. https://doi.org/10.1002/2015JA022089

Collinson, G., Wilson III, L. B., Omidi, N., Sibeck, D., Espley, J., Fowler, C. M., Mitchell, D., Grebowsky, J., Mazelle, D., … Jakosky, B. (2018). Solar wind induced waves in the skies of mars: Ionospheric compression, energization, and escape resulting from the impact of ultralow frequency magnetosonic waves generated upstream of the Martian bow shock. *J. Geophys. Res.: Space Phys.*, *123*(9), 7241–7256. https://doi.org/10.1029/2018JA025414

Connerney, J. E. P., Espley, J., Lawton, P., Murphy, S., Odom, J., Oliversen, R., and Sheppard, D. (2015). The MAVEN magnetic field investigation. *Space Sci. Rev.*, *195*(1-4), 257–291. https://doi.org/10.1007/s11214-015-0169-4

Ergun, R. E., Andersson, L., Peterson, W. K., Brain, D., Delory, G. T., Mitchell, D. L., Lin, R. P., and Yau, A. W. (2006). Role of plasma waves in mars' atmospheric loss. *Geophys. Res. Lett.*, *33*(14), L14103. https://doi.org/10.1029/2006GL025785

Espley, J. R., Cloutier, P. A., Brain, D. A., Crider, D. H., and Acuña, M. H. (2004). Observations of low-frequency magnetic oscillations in the Martian magnetosheath, magnetic pileup region, and tail. *J. Geophys. Res.: Space Phys.*, *109*(A7), A07213. https://doi.org/10.1029/2003JA010193

Fowler, C. M., Andersson, L., Ergun, R. E., Harada, Y., Hara, T., Collinson, G., Peterson, W. K., Espley, J., Halekas, J., … Jakosky, B. M. (2018). MAVEN observations of solar wind-driven magnetosonic waves heating the Martian dayside ionosphere. *J. Geophys. Res.: Space Phys.*, *123*(5), 4129–4149. https://doi.org/10.1029/2018JA025208

Fowler, C. M., Agapitov, O. V., Xu, S., Mitchell, D. L., Andersson, L., Artemyev, A., Espley, J., Ergun, R. E., and Mazelle, C. (2020). Localized heating of the Martian topside ionosphere through the combined effects of magnetic pumping by large-scale magnetosonic waves and pitch angle diffusion by whistler waves. *Geophys. Res. Lett.*, *47*(5), e2019GL086408. https://doi.org/10.1029/2019GL086408

Fowler, C. M., Hanley, K. G., McFadden, J. P., Chaston, C. C., Bonnell, J. W., Halekas, J. S., Espley, J. R., DiBraccio, G. A., Schwartz, S. J., … Lillis, R. J. (2021). MAVEN observations of low frequency steepened magnetosonic waves and associated heating of the Martian nightside ionosphere. *J. Geophys. Res.: Space Phys.*, *126*(10), e2021JA029615. https://doi.org/10.1029/2021JA029615

Guo, Z. Z., Liu, Y. Y., Fu, H. S., Cao, J. B., Xu, Y., Wang, Z., Yu, Y., He, R. J., Liu, X. Y., and Zhang, W. Z. (2022). First observation of lower hybrid drift waves at the edge of the current sheet in the Martian magnetotail. *Astrophys. J.*, *933*(2), 128. https://doi.org/10.3847/1538-4357/ac722b

Halekas, J. S., Taylor, E. R., Dalton, G., Johnson, G., Curtis, D. W., McFadden, J. P., Mitchell, D. L., Lin, R. P., and Jakosky, B. M. (2015). The solar wind ion analyzer for MAVEN. *Space Sci. Rev.*, *195*(1-4), 125–151. https://doi.org/10.1007/s11214-013-0029-z

Harada, Y., Ruhunusiri, S., Halekas, J. S., Espley, J., DiBraccio, G. A., McFadden, J. P., Mitchell, D. L., Mazelle, C., Collinson, G., … Jakosky, B. M. (2019). Locally generated ULF waves in the Martian magnetosphere: MAVEN observations. *J. Geophys. Res.: Space Phys.*, *124*(11), 8707–8726. https://doi.org/10.1029/2019JA027312

Hoppe, M. M., and Russell, C. T. (1983). Plasma rest frame frequencies and polarizations of the low-frequency upstream waves: ISEE 1 and 2 observations. *J. Geophys. Res.*, *88*(A3), 2021–2027. https://doi.org/10.1029/JA088iA03p02021

Horne, R. B., Thorne, R. M., Glauert, S. A., Meredith, N. P., Pokhotelov, D., and Santolík, O. (2007). Electron acceleration in the Van Allen radiation belts by fast magnetosonic waves. *Geophys. Res. Lett.*, *34*(17), L17107. https://doi.org/10.1029/2007GL030267

Jakosky, B. M., Lin, R. P., Grebowsky, J. M., Luhmann, J. G., Mitchell, D. F., Beutelschies, G., Priser, T., Acuna, M., Andersson, L., … Zurek, R. (2015). The

Mars atmosphere and volatile evolution (MAVEN) mission. *Space Sci. Rev.*, *195*(1), 3–48. https://doi.org/10.1007/s11214-015-0139-x

Jian, L. K., Russell, C. T., Luhmann, J. G., Strangeway, R. J., Leisner, J. S., and Galvin, A. B. (2009). Ion cyclotron waves in the solar wind observed by *stereo* near 1 AU. *Astrophys. J.*, *701*(2), L105–L109. https://doi.org/10.1088/0004-637X/701/2/L105

Jian, L. K., Russell, C. T., Luhmann, J. G., Anderson, B. J., Boardsen, S. A., Strangeway, R. J., Cowee, M. M., and Wennmacher, A. (2010). Observations of ion cyclotron waves in the solar wind near 0.3 AU. *J. Geophys. Res.: Space Phys.*, *115*(12), A12115. https://doi.org/10.1029/2010JA015737

Kintner, P. M., Arnoldy, R., Pollock, C., Moore, T., Holtet, J., Deehr, C., and Moen, J. (1997). The SCIFER Sounding Rocket Experiment. In *European Rocket and Balloon Programmes and Related Research*, volume 397 of *ESA Special Publication*, 343.

Langlais, B., Purucker, M. E., and Mandea, M. (2004). Crustal magnetic field of mars. *J. Geophys. Res.: Planets*, *109*(E2), E02008. https://doi.org/10.1029/2003JE002048

Langlais, B., Thébault, E., Houliez, A., Purucker, M. E., and Lillis, R. J. (2019). A new model of the crustal magnetic field of mars using mgs and maven. *J. Geophys. Res.: Planets*, *124*(6), 1542–1569. https://doi.org/10.1029/2018JE005854

Li, J. X., Bortnik, J., Thorne, R. M., Li, W., Ma, Q. L., Baker, D. N., Reeves, G. D., Fennell, J. F., Spence, H. E., … Blake, J. B. (2016). Ultrarelativistic electron butterfly distributions created by parallel acceleration due to magnetosonic waves. *J. Geophys. Res.: Space Phys.*, *121*(4), 3212–3222. https://doi.org/10.1002/2016JA022370

Li, X. Z., Rong, Z. J., Fraenz, M., Zhang, C., Klinger, L., Shi, Z., Gao, J. W., Dunlop, M. W., and Wei, Y. (2023). Two types of Martian magnetotail current sheets: Maven observations of ion composition. *Geophys. Res. Lett.*, *50*(2), e2022GL102630. https://doi.org/10.1029/2022GL102630

Liu, D., Yao, Z. H., Wei, Y., Rong, Z. J., Shan, L. C., Arnaud, S., Jared, E., Wei, H. Y., and Wan, W. X. (2020). Upstream proton cyclotron waves: occurrence and amplitude dependence on IMF cone angle at Mars — from MAVEN observations. *Earth Planet. Phys.*, *4*(1), 51–61. https://doi.org/10.26464/epp2020002

Liu, K. J., Gary, S. P., and Winske, D. (2011). Excitation of magnetosonic waves in the terrestrial magnetosphere: Particle-in-cell simulations. *J. Geophys. Res.: Space Phys.*, *116*(A7), A07212. https://doi.org/10.1029/2010JA016372

Liu, K. J., Min, K., Feng, B., and Wang, Y. (2020). Excitation of oxygen ion cyclotron harmonic waves in the inner magnetosphere: Hybrid simulations. *Geophys. Res. Lett.*, *47*(20), e2020GL090575. https://doi.org/10.1029/2020GL090575

Ma, Q., Li, W., Bortnik, J., Kletzing, C. A., Kurth, W. S., Hospodarsky, G. B., and Wygant, J. R. (2019). Global survey and empirical model of fast magnetosonic waves over their full frequency range in Earth's inner magnetosphere. *J. Geophys. Res.: Space Phys.*, *124*(12), 10270–10282. https://doi.org/10.1029/2019JA027407

McFadden, J. P., Kortmann, O., Curtis, D., Dalton, G., Johnson, G., Abiad, R., Sterling, R., Hatch, K., Berg, P., … Jakosky, B. (2015). MAVEN suprathermal and thermal ion compostion (STATIC) instrument. *Space Sci. Rev.*, *195*(1-4), 199–256. https://doi.org/10.1007/s11214-015-0175-6

Means, J. D. (1972). Use of the three-dimensional covariance matrix in analyzing the polarization properties of plane waves. *J. Geophys. Res.*, *77*(28), 5551–5559. https://doi.org/10.1029/JA077i028p05551

Min, K., Denton, R. E., Liu, K. J., Gary, P. S., and Spence, H. E. (2017). Ion bernstein instability as a possible source for oxygen ion cyclotron harmonic waves. *J. Geophys. Res.: Space Phys.*, *122*(5), 5449–5465. https://doi.org/10.1002/2017JA023979

Min, K., Liu, K. J., Wang, X. Y., Chen, L. J., and Denton, R. E. (2018). Fast magnetosonic waves observed by Van Allen probes: Testing local wave excitation mechanism. *J. Geophys. Res.: Space Phys.*, *123*(1), 497–512. https://doi.org/10.1002/2017JA024867

Mitchell, D. L., Mazelle, C., Sauvaud, J. A., Thocaven, J. J., Rouzaud, J., Fedorov, A., Rouger, P., Toublanc, D., Taylor, E., … Jakosky, B. M. (2016). The MAVEN solar wind electron analyzer. *Space Sci. Rev.*, *200*(1-4), 495–528. https://doi.

org/10.1007/s11214-015-0232-1

Nagy, A. F., Winterhalter, D., Sauer, K., Cravens, T. E., Brecht, S., Mazelle, C., Crider, D., Kallio, E., Zakharov, A., ... Trotignon, J. G. (2004). The plasma environment of mars. *Space Sci. Rev.*, *111*(1), 33–114. https://doi.org/10.1023/B:SPAC.0000032718.47512.92

Ni, B. B., Zou, Z. Y., Fu, S., Cao, X., Gu, X. D., and Xiang, Z. (2018). Resonant scattering of radiation belt electrons by off-equatorial magnetosonic waves. *Geophys. Res. Lett.*, *45*(3), 1228–1236. https://doi.org/10.1002/2017GL075788

Øieroset, M., Mitchell, D. L., Phan, R. D., Lin, R. P., Crider, D. H., and Acuña, M. H. (2004). The magnetic field pile-up and density depletion in the Martian magnetosheath: A comparison with the plasma depletion layer upstream of the Earth's magnetopause. In D. Winterhalter, et al. (Eds.), *Mars' Magnetism and Its Interaction with the Solar Wind* (pp. 185-202). Dordrecht: Springer. https://doi.org/10.1007/978-0-306-48604-3_4

Ruhunusiri, S., Halekas, J. S., Connerney, J. E. P., Espley, J. R., McFadden, J. P., Larson, D. E., Mitchell, D. L., Mazelle, C., and Jakosky, B. M. (2015). Low-frequency waves in the Martian magnetosphere and their response to upstream solar wind driving conditions. *Geophys. Res. Lett.*, *42*(21), 8917–8924. https://doi.org/10.1002/2015GL064968

Russell, C. T., Luhmann, J. G., Schwingenschuh, K., Riedler, W., and Yeroshenko, Y. (1990). Upstream waves at Mars: Phobos observations. *Geophys. Res. Lett.*, *17*(6), 897–900. https://doi.org/10.1029/GL017i006p00897

Shprits, Y. Y. (2009). Potential waves for pitch-angle scattering of near-equatorially mirroring energetic electrons due to the violation of the second adiabatic invariant. *Geophys. Res. Lett.*, *36*(12), L12106. https://doi.org/10.1029/2009GL038322

Shprits, Y. Y. (2016). Estimation of bounce resonant scattering by fast magnetosonic waves. *Geophys. Res. Lett.*, *43*(3), 998–1006. https://doi.org/10.1002/2015GL066796

Su, Z. P., Liu, N. G., Gao, Z. L., Wang, B., Zheng, H. N., Wang, Y. M., and Wang, S. (2020). Rapid landau heating of Martian topside ionospheric electrons by large-amplitude magnetosonic waves. *Geophys. Res. Lett.*, *47*(20), e2020GL090190. https://doi.org/10.1029/2020GL090190

Teng, S., Li, W., Tao, X., Ma, Q., Wu, Y., Capannolo, L., Shen, X. C., and Gan, L. (2019). Generation and characteristics of unusual high frequency EMIC waves. *Geophys. Res. Lett.*, *46*(24), 14230–14238. https://doi.org/10.1029/2019GL085220

Teng, S., Liu, N., Ma, Q., Tao, X., and Li, W. (2021). Direct observational evidence of the simultaneous excitation of electromagnetic ion cyclotron waves and magnetosonic waves by an anisotropic proton ring distribution. *Geophys. Res. Lett.*, *48*(8), e2020GL091850. https://doi.org/10.1029/2020GL091850

Tsurutani, B. T., Falkowski, B. J., Pickett, J. S., Verkhoglyadova, O. P., Santolik, O.,

and Lakhina, G. S. (2014). Extremely intense ELF magnetosonic waves: A survey of polar observations. *J. Geophys. Res.: Space Phys.*, *119*(2), 964–977. https://doi.org/10.1002/2013JA019284

Vignes, D., Mazelle, C., Rme, H., Acuña, M. H., Connerney, J. E. P., Lin, R. P., Mitchell, D. L., Cloutier, P., Crider, D. H., and Ness, N. F. (2000). The solar wind interaction with Mars: Locations and shapes of the bow shock and the magnetic pile-up boundary from the observations of the MAG/ER experiment onboard Mars Global Surveyor. *Geophys. Res. Lett.*, *27*(1), 49–52. https://doi.org/10.1029/1999GL010703

Wang, J., Lee, L. C., Xu, X., Cao, J. B., Yu, J., Chang, Q., Xu, Q., and Xu, J. (2020). Plasma and magnetic-field structures near the Martian induced magnetosphere boundary. I. plasma depletion region and tangential discontinuity. *Astron. Astrophys.*, *642*, A34. https://doi.org/10.1051/0004-6361/201936201

Wang, J., Yu, J., Xu, X. J., Cui, J., Cao, J. B., Ye, Y. D., Xu, Q., Wang, M., Zhou, Z. L., ... Wang, X. (2021). MAVEN observations of magnetic reconnection at Martian induced magnetopause. *Geophys. Res. Lett.*, *48*(21), e2021GL095426. https://doi.org/10.1029/2021GL095426

Wang, J., Yu, J., Chen, Z. Z., Xu, X. J., Cui, J., and Cao, J. B. (2023). Local generation of magnetosonic waves by ring beam hot protons in the Martian ionosphere. *Geophys. Res. Lett.*, *50*(9), e2023GL102911. https://doi.org/10.1029/2023GL102911

Wei, H. Y., Russell, C. T., Zhang, T. L., and Blanco-Cano, X. (2011). Comparative study of ion cyclotron Waves at Mars, Venus and Earth. *Planet. Space Sci.*, *59*(10), 1039–1047. https://doi.org/10.1016/j.pss.2010.01.004

Wei, H. Y., Cowee, M. M., Russell, C. T., and Leinweber, H. K. (2014). Ion cyclotron waves at Mars: Occurrence and wave properties. *J. Geophys. Res.: Space Phys.*, *119*(7), 5244–5258. https://doi.org/10.1002/2014JA020067

Wilson III, L. B. (2016). Low frequency waves at and upstream of collisionless shocks. In A. Keiling, et al. (Eds.), *Low Frequency Waves in Space Plasmas* (pp. 269-291). Washington: AGU. https://doi.org/10.1002/9781119055006.ch16

Wu, Z., Teng, S., Ma, Q., and Tao, X. (2022). A statistical study of pancake pitch angle distribution of low-energy protons and their correlation with magnetosonic waves. *J. Geophys. Res.: Space Phys.*, *127*(5), e2021JA030174. https://doi.org/10.1029/2021JA030174

Yao, F., Yuan, Z. G., Yu, X. D., Wang, D. D., and Ouyang, Z. H. (2020). Analytical fast magnetosonic wave model based on observations of Van Allen probe. *J. Geophys. Res.: Space Phys.*, *125*(10), e2020JA028527. https://doi.org/10.1029/2020JA028527

Yuan, Z. G., Yu, X. D., Huang, S. Y., Qiao, Z., Yao, F., and Funsten, H. O. (2018). Cold ion heating by magnetosonic waves in a density cavity of the plasmasphere. *J. Geophys. Res.: Space Phys.*, *123*(2), 1242–1250. https://doi.org/10.1002/2017JA024919